Dalton Transactions

Accepted Manuscript

This article can be cited before page numbers have been issued, to do this please use: K. Y. Lee, Y. L. Ng, W. S. Wang, Y. P. Ng, W. C. Chan, W. J. Lai, F. Davamani, E. Chitra, W. M. Lim, R. Ganguly, J. Maah, Y. Win and C. H. Ng, *Dalton Trans.*, 2019, DOI: 10.1039/C9DT00506D.

This is an Accepted Manuscript, which has been through the Royal Society of Chemistry peer review process and has been accepted for publication.

Accepted Manuscripts are published online shortly after acceptance, before technical editing, formatting and proof reading. Using this free service, authors can make their results available to the community, in citable form, before we publish the edited article. We will replace this Accepted Manuscript with the edited and formatted Advance Article as soon as it is available.

You can find more information about Accepted Manuscripts in the author guidelines.

Please note that technical editing may introduce minor changes to the text and/or graphics, which may alter content. The journal's standard Terms & Conditions and the ethical guidelines, outlined in our author and reviewer resource centre, still apply. In no event shall the Royal Society of Chemistry be held responsible for any errors or omissions in this Accepted Manuscript or any consequences arising from the use of any information it contains.

ROYAL SOCIETY OF CHEMISTRY

rsc.li/dalton

ROYAL SOCIETY OF CHEMISTRY View Article Online
DOI: 10.1039/C9DT00506D

Dalton Trans.

ARTICLE

Enantiomeric pairs of ternary copper(II) complexes and their Aldol-type condensation products: synthesis, characterization, anticancer and epigenetic properties

nReceived 00th August 2018,
Accepted 00th January 20xx

DOI: 10.1039/x0xx00000x

www.rsc.org/

Khei Yan Lee,[a] Yi Ling Ng,[a] Wai San Wang,[b] Pei Ying Ng,[c] Cheang Wei Chan[d], Lai Jing Wei[d], Fabian Davamani[c], Ebenezer Chitra[c], Wei Meng Lim,[a] Rakesh Ganguly,[e] Mohd Jamil Maah,[f] Foo Win Yip[b] and Chew Hee Ng *[g]

Chiral enantiomers [Cu(phen)(L-ser)(H_2O)]NO_3 **1** and [Cu(phen)(D-ser)(H_2O)]NO_3 **2** (ser = serinato) underwent aldol-type condensation with formaldehyde, with retention of chirality, to yield their respective enantiomeric ternary copper(II) complexes, viz. L- and D-[Cu(phen)(OCA)(H_2O)]NO_3·xH_2O (**3** and **4**; phen = 1,10-phenanthroline; OCA = oxazolidine-4-carboxylate; x = ½, 0–2) respectively. These chiral complexes were characterized by FTIR, elemental analysis, circular dichroism, UV-Visible spectroscopy, fluorescence spectroscopy (FL), molar conductivity measurement, ESI-MS and X-ray crystallography. The crystal structures of **1** and **3** showed both the cationic complexes to have a square pyramidal geometry. These complexes were about nine fold more potent than cisplatin against metastatic MDA-MB-231 breast cancer cells, inducing apoptotic cell death via ROS generation and massive drop in mitochrondrial membrane potential. The results of monitoring EZH1, EZH2 and H3K27me3 revealed that the mode of action of **1**-**4** also involved downregulation of EZH2 and it seemed to be independent of H3K27me3 status.

Introduction

Extensive studies on Aldol-type reaction of binary *bis*(aminoacidato)metal(II) complexes have been extended to those involving ternary aqua(1,10-phenanthroline)(aminoacidato)-copper(II) nitrate complex salts, abbreviated as [Cu(phen)(aa)(H_2O)]NO_3.[1-3] Thus far, the [Cu(phen)(aa)(H_2O)]NO_3 (aa = L- and D-threonine and alanine) and their Aldol-type condensation products have been found to be potent and effective against a wide spectrum of human cancer types *in vitro* and *in vivo* with LC50 (concentration that kills 50% of cells) of between 1-10 µM.[2-6] In fact, anticancer copper(II) complexes are turning out to be potential viable alternatives to platinum complexes, with distinct mechanisms of action. An emerging mechanism of action against cancer cells by metal complexes is *via* epigenetic modulation by targeting histones or epigenetic modification enzymes.[7] At the same time, we have been investigating the biological and anticancer properties of chiral pairs of [Cu(phen)(aa)(H_2O)]X (X = Cl^-; NO_3^-) because chirality can impart a distinct pharmacological effect or bio-recognition.[2,3,6] Many chiral-center enantiomers show significantly different biological activity, pharmacodynamics, pharmacokinetics, and toxicity.[8] Herein, we report the chiral pairs of the precursors [Cu(phen)(ser)(H_2O)]NO_3 and their respective Aldol-type condensation products, together with their anticancer and epigenetic properties.

[a] School of Pharmacy, International Medical University, Bukit Jalil, 57000 Kuala Lumpur, Malaysia. Email: khei.yanlee@student.imu.edu.my; yi.lingng@student.imu.edu.my; weimeng_lim@imu.edu.my.
[b] Department of Chemical Science, Faculty of Science, Universiti Tunku Abdul Rahman, 31900 Kampar, Perak, Malaysia. Email: st_sight-209@hotmail.com; yipfw@utar.edu.my
[c] School of Health Sciences, International Medical University, 57000 Kuala Lumpur, Malaysia. Emails: ngpying@gmail.com; fabian_davamani@imu.edu.my; ebenezer_chitra@imu.edu.my.
[d] Department of Chemistry, University of Malaya, 50603 Kuala Lumpur, Malaysia. Email: estichan91@gmail.com; janice_ljw_92@yahoo.com. Centre for Foundation Studies in Science. Email: mjamil@um.edu.my
[e] Division of Chemistry and Biological Chemistry, Nanyang Technological University, 637371 Singapore. E-mail: rganguly@ntu.edu.sg; Fax: +65 6791-1961; Tel: +65 6592-1698.
[f] Centre for Foundation Studies in Science, University of Malaya, 50603 Kuala Lumpur. Email: mjamil@um.edu.my
[g] Department of Pharmaceutical Chemistry, School of Pharmacy, International Medical University, Bukit Jalil, 57000 Kuala Lumpur, Malaysia.
E-mail: NgChewHee@imu.edu.my ; Fax: +60 3 8656 7229; Tel: +60 3 2731 7483.
† Electronic Supplementary Information (ESI) available: Tables S1-S3 and Figures S1-S3. See DOI: aaaaa/xxxxx

Experimental

Materials and instruments

Copper(II) nitrate trihydrate was obtained from Classic Chemical Sdn Bhd (Systerm). L-serine (98%) and D-serine (98%) were supplied by Acros Organic. 1,10-Phenanthroline monohydrate (99%) was from R&M Chemicals while aqueous formaldehyde (40%) was from LCI Labscan Ltd.

A Perkin Elmer 2400 CHN analyser (Universiti Kebangsaan Malaysia) was used to obtain the elemental analysis (C, H, N) of the copper(II) compounds. The FTIR spectra of these compounds were recorded as KBr pellets in the range 4000–400 cm^{-1} on a Perkin Elmer FT-IR spectrometer. UV-Visible spectroscopic measurement was recorded on a Perkin Elmer Lambda 40 in the range 200–900 nm. A

CON 700 bench top conductivity meter from EUTECH Instruments was used to measure the conductivity of the solvents and methanol–water (1:1 v/v) solutions of the copper(II) compounds (1×10^{-3} M) at 0, 1 and 24 h. Fluorescence spectra of 1×10^{-5} M solutions of the copper(II) compounds, dissolved in 1:1 water–methanol, were obtained at room temperature with a Perkin-Elmer LS55 photoluminescence spectrometer. The fluorescence spectra were recorded at λ_{ex} = 278 nm and λ_{em} from 250 to 500 nm. The circular dichroism spectra of 2.5×10^{-4} M of all the aqueous copper(II) compounds were obtained with a Jasco J-810 spectropolarimeter (Universiti Putra Malaysia) using a 0.1 cm cell at 25°C. ESI-MS spectra of water-methanol (1:1 v/v) solutions of **1** – **4** in the m/z range 50–1000 were obtained using a Thermo Finnigan LCQ benchtop quadrupole ion trap mass spectrometer (National University of Singapore). The capillary temperature for complexes **1**, **2** and **4** was 60°C while that for **3** was 150°C.

Dichloro-dihydrofluorescein diacetate (DCFH-DA), dimethyl sulfoxide (DMSO) and MTT were purchased from Sigma Aldrich, USA. Hoechst® 33342 stain was purchased from ThermoFisher, USA. Dulbecco's modified eagle medium (DMEM) and F12 growth medium were purchased from GIBCO®. MDA-MB-231, MCF10A and Chang Liver cells were purchased from American Type Culture Collection, USA.

Synthesis and characterization of copper(II) compounds

[Cu(phen)(aa)(H_2O)]NO_3·xH_2O **1** and **2**. These compounds (aa: L-ser, **1** and D-ser, **2**; x = 0, ½), with yield of more than 80%, were similarly prepared using the previously published procedure for synthesis of the enantiomeric pair of [Cu(phen)(L-threo)(H_2O)]NO_3 and [Cu(phen)(D-threo)(H_2O)]NO_3[3].

[Cu(phen)(L-ser)(H_2O)]NO_3·½H_2O **1**. FTIR (KBr pellet, cm^{-1}): 3440 [m, ν_{OH} (water)]; 1622, 1344 [m, vs; ν_{COO-} (asym, sym)]; 860, 721 [w, ρ_{CH} (phen)]. ESI-MS(+): m/z 346.8 (100%), 348.8 (46%) (Calc. m/z for [^{63}Cu(phen)(L-ser)]$^+$, 347.2; [^{65}Cu(phen)(L-ser)]$^+$, 349.2). Anal. calc. for $CuC_{15}H_{17}N_4O_{7½}$: C, 41.24; H, 3.92; N, 12.82%. Found: C, 41.30; H, 3.55; N, 13.10. Yield, 85%.

[Cu(phen)(D-ser)(H_2O)]NO_3 **2**. FTIR (KBr pellet, cm^{-1}): 3360 [m, ν_{OH} (water)]; 1622, 1344 [m, vs; ν_{COO-} (asym, sym)]; 860, 721 [w, ρ_{CH} (phen)]. ESI-MS(+): m/z 346.8 (100%), 348.8 (46%) (Calc. m/z for [^{63}Cu(phen)(L-ser)]$^+$, 347.2; [^{65}Cu(phen)(L-ser)]$^+$, 349.2). Anal. calc. for $CuC_{15}H_{16}N_4O_7$: C, 42.11; H, 3.77; N, 13.09%. Found: C, 42.27; H, 3.35; N, 13.17. Yield, 83%.

Aldol-type condensation products. These were obtained from the reactions of **1** and **2** with formaldehyde according to a previous procedure[3]. On heating each reaction mixture at pH 6.5 in a water-bath at 50°C overnight, blue crystals were obtained. Reaction of precursor **1** yielded complex **3** while that of **2** yielded **4**. Complexes **3** and **4** are abbreviated as L-[Cu(phen)(OCA)(H_2O)]NO_3·H_2O and D-[Cu(phen)(OCA)(H_2O)]-NO_3·2H_2O.

L-[Cu(phen)(OCA)(H_2O)]NO_3·H_2O **3**. FTIR (KBr pellet, cm^{-1}): 3416 [m, ν_{OH} (water)]; 1626, 1337 [m, vs; ν_{COO-} (asym, sym)]; 852, 721 [w, ρ_{CH} (phen)]. ESI-MS(+): m/z 358.9 (100%), 360.9 (46%) (Calc. m/z for L-[^{63}Cu(phen)(OCA)]$^+$, 359.2; L-[^{65}Cu(phen)(OCA)]$^+$, 361.2). Anal. calc. for $CuC_{16}H_{18}N_4O_8$: C, 41.97; H, 3.96; N, 12.24%. Found: C, 42.18; H, 3.62; N, 12.95. Yield, 60%.

D-[Cu(phen)(OCA)(H_2O)]NO_3·2H_2O **4**. FTIR (KBr pellet, cm^{-1}): 3397 [m, ν_{OH} (water)]; 1632, 1337 [m, vs; ν_{COO-} (asym, sym)]; 852, 721 [w, ρ_{CH} (phen)]. ESI-MS(+): m/z 358.9 (100%), 360.9 (46%) (Calc. m/z for D-[^{63}Cu(phen)(OCA)]$^+$, 359.2; D-[^{65}Cu(phen)(L-ser)]$^+$, 361.2). Anal. calc. for $CuC_{16}H_{20}N_4O_8$: C, 40.38; H, 4.23; N, 11.77%. Found: C, 40.46; H, 4.54; N, 11.95. Yield, 58%.

X-ray crystal structure determinations

After repeated attempts suitable blue crystals of **1** ($C_{15}H_{16}CuN_4O_7$; dimensions 0.340 mm x 0.340 mm x 0.380 mm) and **3** ($C_{16}H_{18}CuN_4O_8$) were obtained for X-ray crystallography. Crystals of **1** and **3** were mounted on quartz fibres. Bruker APEX3 diffractometer system was used to collect X-ray intensity data, using MoKα radiation λ = 0.71073 Å with the SMART suite of programs.[9a] All data were processed and corrected for Lorentz and polarization effects with SAINT and for absorption effects with SADABS.[9b] The structure was solved by direct method to locate the heavy atoms, followed by difference maps for the light, non-hydrogen atoms and refinement were carried out with the SHELXTL-2017/1.[9c]. Hydrogen atoms were either located directly from the difference maps and refined freely, or placed in calculated positions and refined with a riding model. All non-hydrogen atoms were given anisotropic displacement parameters in the final model.

The integration of the X-ray intensity data for **1**, using a triclinic unit cell, yielded a total of 11008 reflections to a maximum θ angle of 27.21° (0.78 Å resolution), of which 5396 were independent (average redundancy 3.165, completeness = 99.1%, R_{int} = 3.01%, R_{sig} = 3.27%) and 3294 (94.71%) were greater than 2σ(F^2). The final cell constants of *a* = 7.4893(3) Å, *b* = 9.7967(4) Å, *c* = 12.1077(5) Å, α = 97.4994(16)°, β = 106.9521(16)°, γ = 107.5688(16)°, volume = 786.51(6) Å^3, are based upon the refinement of the XYZ-centroids of reflections above 20 σ(I). Data were corrected for absorption effects using the Multi-Scan method (SADABS). The ratio of minimum to maximum apparent transmission was 0.827. The calculated minimum and maximum transmission coefficients (based on crystal size) are 0.6100 and 0.6400. The structure was solved and refined using the Bruker SHELXTL Software Package, using the space group P -1, with Z = 2 for the formula unit, $C_{15}H_{16}CuN_4O_7$. The final anisotropic full-matrix least-squares refinement on F^2 with 266 variables converged at R1 = 4.01%, for the observed data and wR2 = 9.91% for all data. The goodness-of-fit was 1.072. The largest peak in the final difference electron density synthesis was 0.424 e^-/Å^3 and the largest hole was -0.525 e^-/Å^3 with an RMS deviation of 0.094 e^-/Å^3. On the basis of the final model, the calculated density was 1.807 g/cm^3 and F(000), 438 e^-.

The integration of the data for **3** using an orthorhombic unit cell yielded a total of 19885 reflections to a maximum θ angle of 28.91° (0.76 Å resolution), of which 5710 were independent (average redundancy 5.010, completeness = 100.0%, Rint = 3.93%, Rsig = 3.22%) and 5087 (89.09%) were greater than 2σ(F^2). The final cell constants of a = 6.6836(3) Å, b = 12.2756(4) Å, c = 21.8809(8) Å, volume = 1795.22(12) Å^3, are based upon the refinement of the XYZ-centroids of 6955 reflections above 20 σ(I) with 4.988° < 2θ < 57.82°. Data were corrected for absorption effects using the Multi-Scan method (SADABS). The ratio of minimum to maximum apparent transmission was 0.772. The calculated minimum and maximum

View Article Online
DOI: 10.1039/C9DT00506D

transmission coefficients (based on crystal size) are 0.6300 and 0.9050.

The structure was solved and refined using the Bruker SHELXTL Software Package, using the space group P 2_1 2_1 2_1, with Z = 4 for the formula unit, $C_{16}H_{18}CuN_4O_8$. The final anisotropic full-matrix least-squares refinement on F^2 with 275 variables converged at R1 = 3.16%, for the observed data and wR2 = 9.26% for all data. The goodness-of-fit was 1.081. The largest peak in the final difference electron density synthesis was 0.601 e-/Å^3 and the largest hole was -0.649 e-/Å^3 with an RMS deviation of 0.276 e-/Å^3. On the basis of the final model, the calculated density was 1.694 g/cm^3 and F(000), 940 e-.

Crystallographic data for the copper(II) compounds (**1** and **3**) have been deposited with the Cambridge Crystallographic Data Centre (CCDC) as CCDC numbers 1863283 and 1863287.

General procedures for biological studies

NCI-modified MTT assay. The NCI-modified MTT assay was carried out using a previous procedure.[10] The cells (MDA-MB-231, MCF10A and Chang Liver cells) were treated for 48 h with increasing concentration of complexes **1 – 4** (0.1, 2.5, 5, and 10 μM) and cisplatin (10, 30, 60, 90 and 120 μM) as positive control. GI_{50} values (the concentration of the metal complex causing 50% growth inhibition), TGI value (the concentration of the complex causing 0% cell growth), and LC_{50} (the concentration of the complex causing 50% cell death) were obtained from dose–response curves which were plots of percentage cell growth versus concentration of test compound.

Formulae for calculating percentage cell growth are given below.

$$\frac{T_i - T_z}{C - T_z} \times 100 \quad \text{for concentrations for which } T_i < T_z$$

$$\frac{T_i - T_z}{T_z} \times 100 \quad \text{for concentrations for which } T_i \geq T_z$$

where T_z = OD at t = 0, T_i = OD of treated sample and C = OD of untreated sample.

Morphological studies. MDA-MB-231 cells were seeded at a density of 3 x 10^4 cells/mL in 24-well plates and incubated for 48 hours at 37°C in 5% CO_2 incubator. Cells were treated with increasing concentration of each of the copper(II) complexes **1 – 4** (0.1, 2.5, 5, 10 μM) incubated for 48 h. After 48 hours of treatment with test compounds, Hoechst® 33342 stain was added to the cells according to the manufacturer's protocol (Thermofisher) and the cells were observed under fluorescence microscope and photographed to record changes in nuclear morphology.

Apoptosis analysis using annexin V-FITC/PI double staining. MDA-MB-231 cells treated for 48 h with increasing concentration of each of the complexes **1 – 4** (0.1, 2.5, 5 and 10 μM) for 48 h and analysed with flow cytometry to investigate the induction of apoptosis/necrosis as described previously.[10]

Cell cycle analysis. MDA-MB-231 cells were seeded into a series of 60-mm petri dishes at a density 1 × 10^5 cells per dish and incubated overnight. Old media from these dishes were replaced by fresh media with or without complexes **1 – 4** (0.1, 2.5, 5, and 10 μM) before incubating for another 48 h. Then, the cells from each dish were harvested and the resultant pellet so obtained was fixed with 1 mL ice-cold 70% ethanol and stored overnight at 4°C. Each cell pellet of cells was washed twice with 1 mL PBS before centrifuging at 3000 rpm for 5 min to remove excessive ethanol. Then, 500 μL staining solution (20 μg/mL PI and 15 μg/mL RNase) was added to each pellet, and the resultant mixture was incubated at room temperature for a further 15 min. The samples were analyzed by passage through a FACS Calibur employing the BD CellQuest Pro software.

p-nitrosodimethyl-aniline (PNDA) assay. A total volume of 141.6 μL borate buffer solution (33 mM at pH 7.5), 90 μL copper(II) complexes (100 μM), 18 μL H_2O_2 (60 mM) and 50.4 μL PNDA (42 μM) were added sequentially into 96 well transparent plates. The absorbance readings at 440 nm were taken immediately and at every 5 minutes for 4 hours upon the addition of PNDA using the microplate reader (SpectraMax). To quantify the amount of hydroxyl radicals produced by the reaction of the copper(II) complexes and cisplatin with hydrogen peroxide in phosphate–NaCl buffer at pH 7.5, a previously reported PNDA assay was used.[4] The percentage bleaching of the PNDA by the hydroxyl radicals produced was calculated by using the formula, % Bleaching of PNDA = 100 x (A_o - A_t)/A_o where A_o = absorbance of sample with PNDA at 440 nm at t = 0 while A_t = absorbance of sample with PNDA at 440 nm at any time, t.

DCFH-DA assay. MDA-MB-231 cells were seeded at a density of 1 × 10^4 cells/mL in 100 μL medium per well in both 96-well flat bottom black tissue culture plates (SPL, Korea) and 96-well flat bottom transparent tissue culture plates, followed by incubation at 37 °C in a 5% CO_2 incubator overnight. Old media were removed and media with or without complexes **1 – 4** (0.1, 2.5, 5, and 10 μM) were added. All the plates were incubated at 37°C in a 5% CO_2 incubator for 24 h. After the treatment period, old media from 96-well black culture plate were removed. Each well was treated with 100 μL PBS containing DCFH-DA (10 μM), and the plate was gently tapped. The plate was then incubated at 37 °C for 30 min, and the optical density of each well was read at 485 nm with background subtraction at 535 nm by using an ELISA plate reader.

Additionally, in the 96-well transparent tissue culture plate, 20 μL of MTT solution (5 mg/mL) was added to each well, and the plate was further incubated for 4 h. Then, DMSO (80 μL) was added to each well to dissolve the formazan crystals formed. The optical density of of each well was read at 570 nm with background subtraction at 630 nm. The cell viability, normalization, and ROS fold change were then calculated with the formulae listed below by using Microsoft Excel.

$$\text{Percentage of cell viability} = \frac{\text{Average optical density of sample}}{\text{Average optical density of control}} \times 100$$

$$\text{Normalization} = \frac{\text{Average optical density of sample}}{\text{Percentage of viability}} \times 100$$

$$\text{ROS fold change} = \frac{\text{ROS generated from sample}}{\text{ROS generated from control}} \times 100$$

JC-1 mitochondrial membrane potential determination. MDA-MB-231 cells were seeded at 1×10^4 cells in two series of 60-mm tissue culture petri dishes and were incubated at 37°C in a 5% CO_2 incubator overnight. The cells were then treated with or without complexes **1 – 4** (0.1, 2.5, 5, and 10 μM). After 48-h incubation, the treated cells were harvested. The cells were stained using a Mitochondrial Membrane Potential (MMP) Detection Kit containing the JC-1 dye (Becton–Dickinson, USA) according to the manufacturer's instructions. The fluorescence signals of the stained cells were measured by FACSCalibur, and the data collected were analyzed by BD CellQuest Pro software. Microsoft Excel was used to calculate the mitochondrial membrane potential using the formula below.

$$\text{Mitochondria membrane potential} = \frac{\text{R2 Region (Red fluorescence signal)}}{\text{R3 Region (Green fluorescence signal)}}$$

Epigenetic studies (EZH1, EZH2, H3K27me3). The MDA-MB-231 and T47D breast cancer cells were seeded into 6 cm tissue culture dishes. Subsequently, the cells were treated with copper(II) complexes dissolved in PBS media (using their LC50 values) and incubated for 48 hours. The protein lysate was harvested by using lysis buffer and the protein concentration was quantified using Bradford reagent assay. For western blot assay, the sodium dodecyl sulfate-polyacrylamide page was used for protein separation and equal amount of protein sample was loaded into each lane. Once the separation has completed, the protein was transferred into polyvinylidene fluoride (PVDF) membrane using semi dry blot. Next, the membrane was blocked by using 5% w/v bovine serum albumin in phosphate buffer saline with 0.1% v/v Tween 20 (5% BSA-PBST) for an hour. The primary antibodies for EZH2, H3k27Me3 (Cell Signalling Technology) and EZH1 (antibodies-online) respectively were diluted according to the manufacturer recommended concentration and added into the blot to incubate overnight at 4°C. On the next day, the blot was washed with PBST and followed by incubation of secondary antibody-HRP conjugated goat-anti-^{rabbit} or goat-anti-mouse (Bio-Rad Laboratories) in 5% BSA-PBST for an hour. Finally, the membrane was washed with PBST and added with ECL substrate for viewing using Biorad® image lab system.

Statistical analysis. Student t-test was performed to check for significance. A calculated value of $p < 0.05$ was considered statistically significant.

Results and discussion

Synthesis of 1 – 4 and crystal structure analysis 1 and 3.

Under non-basic conditions, the aqueous solutions of the chiral copper(II) complex salts, $[Cu(phen)(L\text{-}ser)(H_2O)]NO_3{\cdot}½H_2O$ or $[Cu(phen)(L\text{-}ser)(H_2O)]NO_3$ **1** and $[Cu(phen)(D\text{-}ser)(H_2O)]NO_3$ **2** reacted with formaldehyde (HCHO) to yield their respective products **3** and **4**.

Crystal structure of 1. Repeated attempts at synthesising **1** was able to yield good crystals of **1** without lattice water. Structural analysis of this sample of **1** shows that it crystallises into the acentric space group *P*1, showing it to be chiral. Each molecule of **1** consists of a cationic complex and an anionic nitrate counter ion (Fig. 1). In the cationic complex, the copper(II) atom has a square pyramidal environment with its basal plane formed by N_3O-ligating atoms of two bidentate ligands, L-serinate (Cu1-O1, 1.934(4) Å; Cu1-N1, 1.998(5) Å) and phen (Cu1-N2, 2.027(5) Å; Cu1-N3, 2.013(5) Å). A water molecule occupies the apical position of the square pyramid with a long Cu1-O7 bond length of 2.275(3) Å. The geometry and the bond lengths about Cu(II) in **1** are similar to those of analogous $[Cu(phen)(aa)(H_2O)]^+$ cations (aa = α-dimethylglycine, DL-alanine).[4] The coordinated L-serinate in **1** has one stereogenic centre at its α-carbon atom (i.e. C2 atom) with **S** absolute configuration. Thus, **1** can be abbreviated as $[Cu(phen)(L\text{-}ser)(H_2O)]NO_3$. Crystallographic data and selected bond lengths and angles are shown in ESI Table S1.1 and S1.2.†

(Fig. 1 here)

Crystal structure of 3. Crystal structure analysis shows **3** to have a chiral space group P 21 21 21. It consists of a cationic complex with a nitrate counter ion. The cationic complex has a square pyramidal geometry about the copper(II) atom, which is formed from coordination of two bidentate ligands, oxazolidine-4-carboxylate (OCA) anion (Cu1-O1, 1.9465(12) Å; Cu1-N1, 2.0002(15) Å) and phen (Cu1-N2, 2.0253(14) Å; Cu1-N3, 1.9827(14) Å), and a water molecule (Cu1-O4, 2.2808(15) Å) (Fig. 2). There is also a lattice water molecule. Thus, **3** can be formulated as $L\text{-}[Cu(phen)(OCA)(H_2O)]NO_3{\cdot}H_2O$. The formation of the oxazolidine ring in **3** is supported by the presence of a set of FTIR triplet peaks, at 1145, 1105 and 1041 cm^{-1}, which is typical of an oxazolidine ring system.[11] The square pyramidal structure of **3** is similar to that of [aquabis(oxazolidine-4-carboxylato)copper(II)], in which the oxazolidine ring was formed from an aldol-type condensation of the α-hydroxymethyl group of the serine moiety of bis(L-serinato)copper(II) with formaldehyde.[12] This oxazolidine ring formation involved an initial N-hydroxymethylation of the chelated L-serine and its subsequent condensation with the adjacent α-hydroxymethyl group.[1]

(Fig. 2 here)

Configurational analysis of the crystal structure of **3** reveals it be chiral, with two stereogenic centres (N1 and C1). These are amino nitrogen N1(R) and the α-carbon C1(S). As product **3** is derived from **1** and both α-carbon atoms of **1** and **3** have the same configuration S, it can be concluded that there is retention of configuration of the α-carbon of the chelated serine after aldol-type condensation with formaldehyde to form the oxazolidine ring. Similarly, the R-enantiomer **2** (i.e. α-carbon has an absolute configuration R) reacted with formaldehyde to yield the R-enantiomer of **4**. This stereospecific retention of configuration of the aldol-type condensation has previously been explained for the reaction of chiral $[Cu(phen)(threo)(H_2O)]NO_3$ (threo = L-threo, D-threo) with formaldehyde.[11] The scheme of the reaction is shown in Fig. 3.

(Fig. 3 here)

In the crystal structure of **3**, there is only one distinct stereoisomer with the same chirality (Fig. 2). It should have two

stereoisomeric $[Cu(phen)(OCA)(H_2O)]^+$ molecules, where the difference is having a coordinated aqua ligand on the opposite side of a stereogenic plane defined by the Cu atom and N_3O atoms (of OCA), as was observed for $[Cu(phen)(5MeOCA)(H_2O)]^+$.[11] This could arise because the apical water molecule is probably labile and can be on either side of the stereogenic plane when they crystallised out of the aqueous solution. However, the crystal structure of **3** only shows one of the stereoisomer, consistent with its chiral space group P212121 and with it been crystallographically pure with its Flack parameter having zero value. Crystallographic data and selected bond lengths and angles of **3** are shown in ESI Tables S2.1 and S2.2.†

Identity of both pairs: 1 & 2 and 3 & 4. Both **1** and **2** contain similar ν_{OH} (water)], ν_{COO-} (asym, sym) and ν_{NH} (amino) peaks of coordinated amino acid and doublet ρ_{CH} peaks of coordinated phen, typical of $[Cu(phen)(aa)(H_2O)]NO_3$.[2-4,6] ESI-MS spectra data (Synthesis and characterization section) confirms the presence of same $[Cu(phen)(ser)]^+$ species, each of which is derived from the easy dissociation of the weakly coordinated water molecule from each cationic complex of **1** and **2**. Elemental analysis data also agree well with both having the same postulated general formula $[Cu(phen)(ser)(H_2O)]$-$NO_3 \cdot xH_2O$. Similarly, the FTIR, ESI-MS and elemental analysis data of **3** and **4** show that this pair have the same characteristic peaks for ν_{OH} (water), ν_{COO-} (asym, sym) and ν_{NH} (amino) peaks of coordinated amino acid and doublet ρ_{CH} peaks of coordinated phen, together with their triplet peaks for oxazolidine ring, and the same postulated formula $[Cu(phen)(OCA)(H_2O)]NO_3 \cdot xH_2O$. The opposite chirality of **1** and **2**, and **3** and **4**, as pair of enantiomers, is established in next sub-section on "Circular dichroism".

Solution properties

Circular dichroism. Before $[Cu(phen)(L\text{-}ser)(H_2O)]$-$NO_3 \cdot ½H_2O$ **1** and $[Cu(phen)(D\text{-}ser)(H_2O)]NO_3$ **2** were reacted with formaldehyde (HCHO), the CD spectra of their aqueous solutions were obtained. Comparison and analysis of the above spectra established **1** and **2** to be a pair of L- and D-enantiomers (Fig. 4). Similarly, analysis of the CD spectra of aqueous solutions of **3** and **4** showed them to be L- and D-enantiomers respectively. From the analysis of these four CD spectra and data in the preceding section, it can be concluded that enantiomeric pair of **1** and **2** reacted with formaldehyde to yield **3** and **4** respectively, with retention of chirality.

(Fig.4 here)

UV-Visible absorption. In the UV spectra of 3×10^{-5} M aqueous solutions of **1**–**4** (Fig. 5; ESI Table S3†), there are two absorption bands at 224–225 and 273 nm, which are due to coordinated phen.[11a,13] The coordinated phen has two absorption bands, one at 227 nm (band A) and that at 264 nm (band B). The latter band has been attributed to a π–π* transition to the lowest-energy singlet excited state 1π–π*.[13,14]

(Fig. 5 here)

The visible spectra of both precursors **1** and **2** show a transition band at 613 nm while those of respective aldol-type condensation products **3** and **4** exhibit a band at 622-623 nm (Fig. 5; ESI Table S3†). These visible bands at λ_{max} 620-623 nm are due to d–d transition, which is similarly observed for aqueous solutions of *bis*(aminoacidato)copper(II), aqua(1,10-phenanthroline)(aminoacidato)copper(II) and both enantiomers of $[Cu(phen)(5MeOCA)(H_2O)]NO_3$ complexes which were obtained from the reaction of formaldehyde with their respective chiral $[Cu(phen)(threo)(H_2O)]NO_3$ precursors.[11,13,14]

Molar conductivity. To investigate the species in solution and their stability, the molar conductivities of 1×10^{-3} M copper(II) complexes **1** – **4** and the precursor compounds in water–methanol (1 : 1 v/v) were obtained at 0, 1 and 24 h (ESI Table S4†). The aqueous solution of $Cu(NO_3)_2$, which was used to synthesise **1** and **2**, has a molar conductivity of ~120 S cm^2 mol^{-1}, which is within the range of typical 2:1 electrolytes.[15] However, the molar conductivities of **1** – **4** are similar (about 50 S cm^2 mol^{-1}) and these values are typical of 1:1 electrolytes.[16] This suggests that these complexes, the enantiomeric pairs of $[Cu(phen)(ser)(H_2O)]NO_3$ and $[Cu(phen)(OCA)(H_2O)]NO_3$, dissociate to yield the copper(II) complex cations and nitrate ions upon dissolution in aqueous solution. These cationic complex species can thus be formulated as $[Cu(phen)(ser)(H_2O)]^+$ (for **1** and **2**) and $[Cu(phen)(OCA)(H_2O)]^+$ (for **3** and **4**) respectively in aqueous solution (chirality symbols are omitted). Within 24 h, the molar conductivities of these four cationic complexes remained practically unchanged, suggesting no dissociation of the chelated amino acid moieties (not shown).

Mass spectra. Analysis of the ESI-MS(+) spectra of water–methanol solutions of **1** – **4** show M^+ ion peaks (100%) and these have been assigned (in the Experimental section) to the presence of $[Cu(phen)(ser)]^+$ (m/z: 346.8 (100%), 348.8 (~46%)) and $[Cu(phen)(OCA)]^+$ (m/z: 358.9 (100%), 360.9 (~44%)) ions with the correct copper isotopic ratios (63Cu and 65Cu) (ESI Fig. S1.1–S1.4†). The $[Cu(phen)(ser)(H_2O)]^+$ and $[Cu(phen)(OCA)(H_2O)]^+$ species were not observed in above mass spectra as the loosely coordinated apical water molecule in the cationic complex could have been easily lost under the ESI-MS ionization conditions.[4,11] In the ESI-MS spectra of complexes **1**, **2** and **4**, the capillary temperature was set at 60°C, and there were no minor m/z peaks due to any dissociation or fragmentation. This is consistent with molar conductivity data which did not support any dissociation of ligand at 24 h storage. However, the ESI-MS spectrum of **3** was obtained at capillary temperature 150°C. Here, minor peaks (<20% each, in peak height) at 274.8, 328.9, 484.9 and 779.7 were also observed. The first two are likely to be due to fragmentation caused by higher capillary temperature while the last two peaks could be due to aggregation, as was previously observed for in ESI-MS(+) of $[Cu(phen)(5MeOCA)]^+$.[11] Based on this ESI-MS data and the molar conductivity data in the previous section, the $[Cu(phen)(ser)(H_2O)]^+$ or $[Cu(phen)(ser)]^+$ and $[Cu(phen)(OCA)(H_2O)]^+$ or $[Cu(phen)(OCA)]^+$ should be the only species in the water–methanol solutions of **1** and **2** pair and **3**

View Article Online
DOI: 10.1039/C9DT00506D

and **4** pair respectively. The breakdown of these species are most unlikely at room temperature.

Fluorescence emission. Irradiation of the free phen and the complexes **1** – **4** with 272 nm light produced similar shaped fluorescence (FL) emission spectra with two merged bands of slightly different intensities (ESI Fig. S2†). The free phen ligand has an intensity of 900 units at λ_{max} of 360 nm while the complexes **1** – **4** have FL emission intensity of less than10 units at λ_{max} in the range 360-365 nm. The substantial FL quenching of the phen (**5**) upon coordination to copper(II) in **1** – **4** have previously been observed for similar Cu(II)-phen complexes.[3,11,17] Interestingly, the intensity of the FL spectra of the two enantiomers of $[Cu(phen)(ser)(H_2O)]NO_3{\cdot}xH_2O$ (**1** and **2**) are very similar while those of the aldol-type condensation products $[Cu(phen)(OCA)(H_2O)]NO_3{\cdot}xH_2O$ (**3** and **4**) are distinctly different and have higher FL emission intensities than the former (by about 2×). Apparently, modification of the chelated ser into the chelated OCA causes enhancement of FL emission.

Anticancer studies

The anticancer studies for **1** – **4** and cisplatin (as positive control) were conducted on the metastatic breast cancer cell line MDA-MB-231 and two normal cell lines, viz. MCF-10A and Chang liver, using NCI-modified MTT assay. To investigate the mode of action of these copper(II) complexes on MDA-MB-231 cells, nuclear morphological observation with microscope, cell cycle and apoptosis analysis with flow cytometer, reactive oxygen studies using PNDA and DCFH-DA, and epigenetic studies on the expression of EZH1, EZH2 and H3K27Me3 were undertaken.

(Table 1 here)

NCI-modified MTT assay. Among the different types of cancer affecting women in Malaysia and worldwide, breast cancer is the most common.[18] Once it progresses to metastasis, survival rate is poor and the mortality rate is about 90%.[19,20] Currently, there is still no effective modality to treat breast cancer when it has advanced to the metastatic stage.[21] Therefore, there is an urgency to develop new drugs against metastatic breast cancer. Consequently, we chose the metastatic MDA-MB-231 breast cancer cell line and two normal cell lines, MCF-10A and Chang Liver, to screen for anticancer property of complexes **1** – **4**. To investigate this, the cells were treated with increasing concentrations of each of these copper(II) complexes for 48 h. From the graphs of percentage growth versus concentration of each copper(II) complex, their GI_{50}, TGI, and LC_{50} values (graphs are not shown) were obtained and these are tabulated in Table 1. This breast cancer cell line was found to be sensitive to all the complexes **1** – **4** (i.e. having high anticancer potency with LC_{50} values in the range 4-9 μM) but it was highly resistant to cisplatin (LC_{50} = 96 μM). However, these complexes were not selective towards MDA-MB-231 over the normal MCF10A and Chang Liver cells. Other similar copper(II) complexes ($[Cu(phen)(aa)(H_2O)]NO_3$ where aa = methylated glycine derivatives) exhibited similar potency towards MDA-MB-231 but had slightly better selectivity (MCF10A:MDA-MB-231 IC_{50} ratios of about 2-3).[22] In spite of this poor *in vitro* selectivity, one of these, $[Cu(phen)(C\text{-}dmg)(H_2O)]NO_3$ (C-dmg = α-dimethylglycine), significantly inhibited tumour growth in nasopharyngeal carcinoma xenograft bearing mice models at doses which were well tolerated without causing significant or permanent toxic side effects.[23] Thus, the poor *in vitro* selectivity might not imply poor *in vivo* selectivity and the toxicity towards some normal cell lines might not be reflected in toxicity to cells in various organ.

Mechanism of action 1-4 on MDA-MB-231

Apoptosis and cell cycle analysis.

The MTT assay results above showed that for copper(II) complexes **1** – **4** merely induced growth inhibition of the MDA-MB-231 cells with very low or no cell death when the treatment concentrations were below 4 μM. Cancer cells treated with 10 μM of each of the copper(II) complexes underwent massive cell death, as suggested by the nearly 100% negative growth. To further investigate the nature of growth inhibition and cell death, cell cycle analysis and annexin V-FITC/PI assay (apoptosis) were performed respectively. Untreated cells have a cell phase distribution of about 1% at SubG1, 65% at G0/G1, 11% at S, and 22% at G2/M (Fig. 6). Cells treated with 0.1 and 2.5 μM of each copper(II) complex did not undergo very significant changes in the cell cycle phase distribution. There was significant increase in cell population at SubG1 phase when cells were treated with 5 μM. A high proportion of cells was in this SubG1 phase (more than 55%) when cells were treated at 10 μM of copper(II) complexes. Cells at SubG1 phase have fragmented DNA, indicative of apoptosis.[24]

(Fig.6 here)

The nature of cell death was then investigated by annexin V-FITC double staining method which allowed the quantification of viable, necrotic and apoptotic cells. Untreated cells after 48 h incubation consisted of mainly viable cells (>80%) with less than 20% apoptotic cells and very minor necrotic cells (Fig. 7). The percentage of apoptotic cells increased when treated with increasing concentration of each copper(II) complex, and it reached about 60-85% when cells were treated with 10 μM. The percentage of necrotic cells remained below 1% at all treatment concentration of copper(II) complexes. Therefore, **1** – **4** induced only apoptotic death of the cancer cells. Further analysis of the data showed that **3** and **4** induced significantly higher apoptotic cell death (e.g more than 80% at 10 μM) than **1** and **2** (only 60-70% at 10 μM). This is also seen in Hoechst staining. However, the chirality of the both pairs (**1** & **2**; **3** & **4**) seemed to have no or insignificant effect on inducing apoptosis. The chiral pairs L- and D-$[Cu(phen)(5MeOCA)(H_2O)]NO_3$ also did not show any effect of chirality on their anticancer property.[11]

(Fig. 7 here)

PNDA assay and hydroxyl radicals. The anticancer property of copper(II) complexes is partially due to their ability to generate additional ROS species in cancer cells to selectively initiate

apoptosis as these cells are believed to be at higher ROS stress and nearer to the threshold of ROS-induced apoptosis.[25] As endogenous hydrogen peroxide (H_2O_2) is found in cancer cells and all cell types in the human body,[26] the amount of hydroxyl radicals produced by the reaction of copper(II) complexes with H_2O_2 in borate buffer at pH 7.5 was monitored by p-nitrosodimethylaniline (PNDA) .[27] The percentage bleaching of the PNDA reagent is proportional to the hydroxyl radicals produced from the reaction of H_2O_2 with the copper(II) complexes (Fig. 8). The reaction was completed by about 120 minutes without any significance difference observed between the L- and D-enantiomers (i.e. **1** and **2**, **3** and 4), suggesting no effect of chirality of the complexes on their rate of reaction with H_2O_2.

(Fig. 8 here)

Intracellular ROS measurement with DCFH-DA. To assess whether **1** – **4** generate ROS in the MDA-MB-231 cells, these cells were treated with different doses (0.1, 2.5, 5 and 10 μM) for 24 h. The ROS levels in the treated cells were detected by flow cytometric analysis using the fluorophore, dichlorofluorescin diacetate (DCFH-DA), which is a well-established compound to detect and quantify intracellular ROS (H_2O_2, ·OH).[22] The generated ROS would oxidise the non-fluorescent dichlorofluorescein (DCFH) to fluorescent DCF and an increase in fluorescent would indicate higher ROS level. The results showed that only the pair of copper(II) complexes, **1** and **2**, induced some increase in intracellular ROS (fold change >1) for 0.1, 2.5 and 5 μM doses while there seemed to be a slight drop in detected ROS in cells treated by similar doses of **3** and **4** (Fig. 9). For cells treated with 10 μM of all complexes for 24 h, there was significant increase in ROS. The lower ROS level detected for cells treated with 0.1 – 5 μM of copper(II) complexes could be due to quenching by the high cellular antioxidants, such as superoxide dismutase and glutathione.[28,29] The copper(II) complexes, at prolonged incubation period (48 h) and/or sufficiently high concentration, could produce ROS to elevate oxidative stress beyond the thresshold level which then led to initiation of apoptosis.[22,30]. ROS-induced apoptosis has also been established for other ROS-generating organic compounds.[31,32] Besides its roles in normal physiological functions and immune system, it is also known that ROS plays a central role in the three main types of apoptosis mediated by mitochondria, death receptors and endoplasmic reticulum.[28] It has been found that copper(II) complexes could induced oxidative nuclear damage by causing difficult-to-repair DNA double strand breaks which then initiate events leading to apoptosis.[22,28,33] The copper(II) complexes could also upset the mitochondria redox homeostasis by increasing the mitochondrial ROS level and depleting the mitochondrial antioxidant, and thereby triggering mitochondrial dysfunction and apoptosis.[29,34] Uptake of copper(II) complexes into mitochondria have been established, and thereby supporting their direct involvement in processes leading to apoptosis.[33]

(Fig.9 here)

Nuclear morphological studies with Hoechst 33342 staining. The cancer cells treated with 0.1-10 μM of **1** – **4** showed increased intensity of blue fluorescence of the Hoechst-stained nuclei and nuclear fragmentation compared with untreated cells (Fig. 10), indicating chromatin condensation, which is one of the morphological characteristics of cells undergoing apoptosis.[28,35] The number of cells decreased at higher concentrations of each complex, indicating loss of viable population due to cell rupture and DNA fragmentation. Both **3** and **4** seemed to have higher toxicity at the lowest concentration compared to **1** and **2**, as evident by the bright blue staining of the nuclei.

(Fig. 10 here)

JC-1 assay and mitochondrial membrane potential

Mitochondria are now considered as an attractive target for anticancer drug development, and this involves compounds having ability to either activate the cell death machinery in cancer cells by inhibiting tumour-specific alterations of the mitochondrial metabolism or by stimulating mitochondrial membrane permeabilization.[36] Copper(II) complexes have potential to be the second type of mitochondria-targeting anticancer compounds as they have been found to decrease the mitochondrial membrane potential of cancer cells.[37-39] To investigate the change in mitochondrial membrane potential ($\Delta\Psi_m$), cationic JC-1 dye was used as JC-1 easily enter the highly polarised mitochondria of healthy cancer cells to form orange aggregates, and they diffuse from inside the mitochondria into the cytoplasm to reform the monomeric, green JC-1 species when the mitochondria become depolarised.[40,41] MDA-MB-231 cells were treated without or with different doses of each of the copper(II) complexes (0.1,2.5, 5 and 10 μM) for 48 h (Fig. 11, Table 2). As low as 2.5 μM of copper(II) complex could cause a massive drop of $\Delta\Psi_m$ by 40 - 60%. It has been postulated that cationic molecules, like the present $[Cu(phen)(aa)(H_2O)]^+$ species in **1** – **4**, are easily attracted to and can accumulate preferentially within the negatively charged mitochondrial matrix which maintains a high negative potential of about -180 mV for electron transport processes.[42] In fact, uptake of such copper(II) complexes into the mitochondria has been experimentally proven.[33] At a treatment concentration of 2.5 μM, MTT assay results merely showed growth inhibition while apoptosis assay showed low increase of apoptotic cells (from about 15% apoptotic cells in control versus about 18-27% in treated cells). At 5 and 10 μM, the complexes could cause almost total loss in $\Delta\Psi_m$. More than 60% of cancer cells have undergone apoptosis after 48 h when treated with 10 μM of each copper(II) complex. These results suggest that the massive drop in $\Delta\Psi_m$ occurred early, and the drop in ΔΨm is in fact one feature of various signalling events in mitochondrial mediated apoptosis.[28] ROS generated by the copper(II) complexes, **1** – **4**, inside the mitochondria could trigger the initiation of this type of apoptosis, and the various events identified include drop in ΔΨm.[28] In fact, lowering of $\Delta\Psi_m$ or perturbance of mitochondrial function with opening of permeability transition pores and release of apoptogenic molecules has been observed in drug-induced apoptosis during cancer treatment.[28,43] Similar loss of $\Delta\Psi_m$ and concomitant cell death of cancer cells via

View Article Online
DOI: 10.1039/C9DT00506D

apoptosis by various copper(II) complexes have been reported by us and others.[10,22,29]

(Fig. 11 here)

Epigenetic study.

Increased levels of enhancer of zeste homolog 2 (EZH2) are associated with negative estrogen receptor (ER(-)) expression and disease progression in breast cancer.[44] In fact, EZH2 is a validated target of numerous types of cancers having aberrant expression of EZH2.[45] The breast cancer cell lines MDA-MB-231, MCF7, and T47D were found to have high expression of EZH2.[44,46,47] In fact, this protein is a marker of aggressive breast cancer.[48] Inhibition of EZH2 methyltransferase activity in cancer cells has been reported to decrease global histone-3 lysine-27 (H3K27) methylation, and decreased cell proliferation, cell cycle arrest, and induction of apoptosis.[45,49] The above review led us to merely investigate the expression of EZH2, EZH1 and H3K27Me3 in MDA-MB-231 (ER(-)) and T47D (ER(+)) breast cancer cells treated with LC50 values of **1**, **2**, **3** or **4** for 48 h.

(Fig. 12 here)

Our results showed that both the breast cancer cell lines had high expression of EZH2 (Fig. 12). In MDA-MB-231 cells treated with **1** – **4**, there was downregulation of EZH2; similar results were obtained for T47D treated cells. However, H3K27Me3 expression seemed to be absent in untreated MDA-MB-231 cells. It seems that the anticancer property of all four copper(II) complexes is associated with downregulation of EZH2 but independent of H3K27Me3 status, unlike other anticancer compounds which downregulated EZH2 with decreased H3K27Me3 expression.[44-47] Similarly, T47D cells treated with **1** – **4** resulted in downregulation of EZH2 (Fig. 12). Contrary to what has been observed so far, the downregulation of EZH2 in MDA-MB-231 by **2** and **3** has resulted in high expression of H3K27Me3. Our literature search was not able to help elucidate such aberrant connection between EZH2 and H3K27me3 expression. Further studies are needed to uncover this contradiction and unravel non-histone methylating role of EZH2. As histone H3 has 12 lysine residues, their methylation status (0, 1, 2 or 3) and their resultant effect may be relevant to the role of EZH2 in regulation of expression of genes.[50]

In contrast to downregulation of EZH2 in both MDA-MB-231 (ER(-)) and T47D (ER(+)) breast cancer cell lines by the chiral pairs **1** and **2**, and chiral pairs **3** and **4**, EZH1 expression was significantly upregulated by all four complexes in the treated MDA-MB-231 cells. On the other hand, the EZH1 upregulation in treated T47D cells was only more distinct for complexes **3** and **4**. Another observed difference in the epigenetic modulation of both cell lines by these complexes was absence or presence of trimethylation of H3K27 which seemed to be affected by the chirality of the complexes. In MDA-MB-231, **2** and **3** seemed to be associated with intense trimethylation of H3K27 while in T47D cells, **1**, **2** and **3** seems to cause intense trimethylation of T47D. The increase of H3K27M23 may be partially explained by the ability of EZH1, a homologue of EZH2, to methylate H3K27.[51] EZH2 is the catalytic subunit of Polycomb repressive complex 2 (PRC2) while EZH1 is the catalytic subunit of PRC1.

Conclusions

The crystal structures of **1** and **3** helped to elucidate how the aldol-type condensation occurred with retention of the chirality of α-carbon of the chelated α-amino acid. The reaction of $[Cu(phen)(threo)(H_2O)_2]NO_3$ (threo = L- & D-isomers) with HCHO also led to retention of the configuration of the α-carbon in the oxazolidine-containing products whereas the reaction of the $[Cu(phen)(ala)(H_2O)]NO_3$ (ala = L- & D-isomers) with HCHO led to racemic oxazolidine-containing products. The mechanism to explain the absence or retention of chirality of the α-carbon of the starting materials, $[Cu(phen)(ser)(H_2O)]NO_3$, to form the reaction products can be extended to similar aldol-type condensation reaction of other $[M(phen)(\alpha\text{-aa})(H_2O)]NO_3$ and the extensively investigated reactions of $M(aa)_2$ (M = metal(II); aa = α-amino acid) with HCHO or other aldehyde.

The greater potency of the **1** – **4** than cisplatin towards metastatic MDA-MB-231 support them as potential alternatives to development of new anticancer therapy for difficult to cure metastatic breast cancer.[52,53]

The mechanistic action of anticancer complexes **1** – **4** are multifactorial, and involves ROS production, lowering of mitochondrial membrane potential and downregulation of EZH2. Although not tested here, DNA damage is another cause of apoptosis. Because of the unusual relationship between the EZH2 downregulation and the increase trimethylation of H3K27, it would be interesting to study further the role of EZH2 in the mode of action of **1** – **4**.

Conflicts of interest

There are no conflicts to declare.

Acknowledgements

This work was supported by Malaysian Ministry of Higher Education grant FRGS/1/2012/SG01/UTAR/02/1, University of Malaya Frontier Research Grant FG036-17AFR, and International Medical University project BP1-01/14(59)2017.

.

Notes and references

1 S. B. Teo, C. H. Ng, E. Horn, E.R. T. Tiekink, *Inorg. Chim Acta*, 1991, **183**, 25.; S. B. Teo, S. G. Teoh, C. H. Ng, H. K. Fun, J. P. Declercq, (1995) *Polyhedron*, 1995, **14**, 1447; S.B. Teo, S. G. Teoh, C. H. Ng, H. K. Fun, J. P. Declercq, *Inorg. Chim Acta*, 2002, **340**, 81.

2 C. H. Ng, W. S. Wang, K. V. Chong, Y. F. Win, K. E. Neoh, H. B. Lee, S. L. San, R. N. Z. Raja Abd Rahman, W. K. Leong, *Dalton Trans*., 2013, **42**, 10233

3 C. H. Ng, W. S. Wang, Y. F. Win, K. E. Neoh, R. Ganguly, H. M. Er, I. H. Ooi, *Transit. Met. Chem*., 2016, **41**, 563.

4 H. L. Seng, W. S. Wang, S. M. Kong, H. K. Alan Ong, Y. F. Win, R. N. Z. Raja Abd. Rahman, M. Chikira, W. K. Leong, M. Ahmad, S. B. Alan Khoo, C. H. Ng, *Biometals*, 2012, **25**, 1061.

5 M. Ahmad, S. N. Suhaimi, T. L. Chu, N. Abdul Aziz, N. K. Mohd Kornain, D. S. Samiulla, K. W. Lo, C. H. Ng, S. B. Alan Khoo *PLosOne* 13(1): e0191295.https:// doi.org/10.1371/journal.pone.0191295

6 P.Y. Ng, C. M. Chye, Y. L. Tiong, C. W. Chan, K. W. Tan, I. H. Ooi, C. H. Ng, *Transit. Met. Chem*., 2018, **43**, 479.
7 C.-H. Leung, L.-J. Liu, K.-H. Leung, D.-L. Ma, *Coord. Chem. Rev*., 2016, **319**, 25.
8 S. R. LaPlante, L. D. Fader, K. R. Fandrick, D. R. Fandrick, O. Hucke, R. Kemper, S. P. F. Miller and P. J. Edwards, *J. Med. Chem*., 2011, **54**, 7005; D. R. P. Almeida, D. M. Gasparro, L. F. Pisterzi, L. L. Torday, A. Varro, J. G. Papp, B. Penke and I. G. Csizmadia, *J. Phys. Chem. A*, 2003, **107**, 5594.
9 (a) SMART version V8.38A; Bruker AXS Inc. Madison, WI, USA 2018; (b) Shledrick, G. M. SADABS; University of Gottingen, Gottingen, Germany, 1996 (c) SHELXTL -2017/1 (Sheldrick, 2017).
10 S. T. Von, H. L. Seng, H. B. Lee, S. W. Ng, M. Chikira, Y. Kitamura, C. H. Ng, *J. Biol. Inorg. Chem*.,2012, **17**, 57.
11 (a) C. H. Ng, W. S. Wang, K. V. Chong, Y. F. Win, K. E. Neo, H. B. Lee, S. L. San, R. N. Z. Raja Abd Rahman, W. K. Leong, *Dalton Trans*., 2013, **42**, 10233; (b) C. H. Ng, T. S. Chong, S. G. Teoh, F. Adams and S. W. Ng, *Dalton Trans*., 2002, 3361; (c) S. B. Teo, C. H. Ng, E. Horn and E. R. T. Tiekink, *Inorg. Chim. Acta*, 1991, **183**, 25.
12 C. H. Ng, Y. T. Lim, M. Moris, S. G. Teoh, *Polyhedron* , 2003, **22**, 521.
13 N. Armoroli, L. De Cola, V. Balzani, J.-P. Sauvage, C. O. Dietrich-Buchecker and J. M. Kern, *J. Chem. Soc., Faraday Trans*., 1992, **88**, 553; M. S. Henry and M. Z. Hoffman, *J. Phys. Chem*., 1979, **83**, 618.
14 C. H. Ng, H. K. Alan Ong, C. W. Kong, K. K. Su and S. W. Ng, *J. Coord. Chem.*, 2006, **59**, 1089.
15 O. F. Ikotun, E. M. Higbee, W. Ouellette and R. P. Doyle, *J. Inorg. Biochem*., 2009, **103**, 1254.
16 C. Bolos, P. C. Christidis, G. Will and L. Wiehl, *Inorg. Chim. Acta*, 1996, **248**, 209.
17 H. L. Seng, H. K. Alan Ong, R. N. Z. Raja Abd Rahman, B. M. Yamin, E. R. T. Tiekink, K. W. Tan, M. J. Maah, I. Caracelli and C. H. Ng, *J. Inorg. Biochem*., 2008, **102**, 1997.
18 R. L. Siegel, K. D. Miller, A. Jemal, 2018. *Cancer J. Clin.,* 2018, **68**,7.
19 A. Stevanovic, P. Lee, N. Wilcken, *Aust. Fam. Physician*, 2006, **35**, 309.
20 J. Ma, H. Lu, S. Wang, B. Chen, Z. Liu, X. Ke, T. Liu, J. Fu*, Int. J. Oncol*., 2015, **46**, 1619.
21 M. Li, Z. Tang, D. Zhang, H. Sun, H. Liu, Y. Zhang, Y. Zhang, X. Chen, *Biomaterials*, 2015, **51**, 161.
22 C. H. Ng, S. M. Kong, Y. L. Tiong, M. J. Maah, N. Sukram, M. Ahmad, Alan S. B. Khoo, *Metallomics*, 2014, **6**, 892.
23 M. Ahmad, S. N. Suhaimi, T. L. Chu, N. Abdul Aziz, N. K. Mohd Kornain, D. S. Samiulla, K. W. Lo, C. H. Ng, Alan S. Khoo, **PLoS ONE**, 2018, **13(1)**: e0191295.
24 M. Kajstura, H. Dorota Halicka, J. Pryjma, Z. Zbigniew Darzynkiewicz, *Cytometry Part A*, 2007, **71A**, 125.
25 B. Halliwell, M.V. Clement, H.L. Lee, *FEBS Lett*. 2000, **486**, 10.
26 C. H. Ng, H. K. Alan Ong, C.W. Kong, K. W. Tan, R. N. Z. Raja Abd. Rahman, B. M. Yamin, S. W. Ng, *Polyhedron*, 2006, **25** 3118.
27 C. Gorrini, I. S. Harris, T. W. Mak, *Nat. Rev. Drug Discov*., 2013, **12**, 931.
28 M. Redza-Dutordoir, D. A. Averill-Bates, *Biochim. Biophys. Acta,* 2016, **1863**, 2977.
29 R. Kachadourian, H. M. Brechbuh, L. Ruiz-Azuara, I.Gracia-Mora, B. J. Day, *Toxicology*, 2010, **268**, 176.
30 X. J. Wu and X. Hua, *Cancer Biol. Ther*., 2007, **6**, 646.
31 K. Li, B. Wang, L. Zheng, K. Yang, Y. Li, M. Hu, D. He, Bioorg. Med. Chem. Lett., 2018, 28, 273
32 Y. Uchihara, K. Tago, H. Taguchi, Y. Narukawa, F. Kiuchi, H. Tamura, M. Funakoshi-Tago, *Biochem. Pharmacol*., 154, 2018, 357.
33 X. Shia, H. Fang, Y. Guo, H. Yuan, Z. Guo, X. Wang, *J. Inorg. Biochem*., 2019, **190**, 38).
34 Nature Nanotechnology, 2019, https://doi-org.ezp2.imu.edu.my/10.1038/s41565-019-0373-6.
35 D. Tarn, C.-J. Yu, J. Lu, Anna Hartz a, Fuyuhiko Tamanoi cd and Jeffrey I. Zink, *Mol. Syst. Des. Eng*., 2017, **2**, 384; Y.-G. Han, S-.C. Liu, T. Zhang, Z. Yang, *Cell Mol. Neurobiol.*, 2011, **31**, 65.
36 S. Fulda, L. Galluzzi, G. Kroemer, Nature Review Drug Discovery, 2010, 9, 447; H. He1, D.-W. Li, L.-Y. Yang, L. Fu, X.-L. Zhu, W.-K. Wong, F.-L. Jiang,, Y. Liu, *Scientific Reports*, 2015, **5**, 13543
37 P. Y. Ng, S. M. Chye, Y. L. Tiong, C. W. Chan, K. W. Tan, I. H. Ooi, C. H. Ng,*Trans. Met. Chem*., 2018, **43**, 479.
38 X. Shi, H. Fang, Y. Guo, H. Yuan, Z. Guo, X. Wang, *J. Inorg. Biochem*., 2019, **190**, 38.
39 J. Deng, P. Yu, Z. Zhang, J. Wang, J. Cai, N. Wu, H. Sun, H. Liang, F. Yang, *Eur. J. Med. Chem*., 2018, **158**,442.
40 H. Hada, C. Honda, H. Tanemura, *Photogr. Sci. Eng*. 1977, **21**, 83.
41 M. Reers, T. W. Smith, L. B. Chen, Biochemistry, 1991, **30**, 4480.
42 M. P. Murphy, R. A. I. Smith, *Annu. Rev. Pharmacol. Toxicol*., 2007, **47**, 629.
43 K. -M. Debatin, *Toxicol. Lett*., 2000, **112–113**, 41.
44 M. E. Gonzalez, X. Li, K. Toy, M. DuPrie, A. C. Ventura, M. Banerjee, M. Ljungman, S. D. Merajver, C. G. Kleer, Oncogene, 2009, **28**, 843.
45 H. Kimberly Kim, W. M. Roberts Charles, *Nat. Med*., 2016, **22** 128.
46 M. Dimri, P.V. Bommi, A.A. Shasrabuddhe, J.D. Khandekar, G.P. Dimri, *Carcinogenesis*, 2010, **31**, 489.
47 C. Gong, S. Yao, A. R. Gomes, E. P. S. Man, H. J. Lee, G. Gong, S. Chang, S. -W. Kim, S. K. Park, J. W. Lee, M. H. Lee, U. S. Khoo, KOHBRA study group, E. W. -F. Lam, *Oncogenesis*, 2016, **5** e214; doi:10.1038/oncsis.2016.23.
48 C. G. Kleer, Q. Cao, S. Varambally, R. Shen, I. Ota, S. A. Tomlins, D. Ghosh, G. A. B. Richard Sewalt, A. P. Otte, D. F. Hayes, M. S. Sabel, D. Livant, S. J. Weiss, M. A. Rubin, A. M. Chinnaiyan, *PNAS*, 2003, **10**, 11606.
49 X. Song, T. Gao, N. Wang, Q. Feng, X. You, Y. Shi, Y. Wei, L. Zhang, L. Yu, *Sci. Rep.*, 2016, **6**, 20864 (DOI: 10.1038/srep20864).
50 K. W. Kuntz, J. E. Campbell, H. Keilhack, R. M. Pollock, S. K. Knutson, M. Porter-Scot, V. M. Richon, C. J. Sneeringer, T. J. Wigle, C. J. Allain, C. R. Majer, M. P. Moyer, R. A. Copeland, R. Chesworth, *J. Med. Chem*., 2016, **59**, 1556.
51 X. Shen, Y. Liu, Yu.-J. Hsu, Y. Fujiwara, J. Kim, X. Mao, G. C. Yuan, S.H. Orkin, Mol. Cell, 2008, **32**, 491–502.
52 P. S. Steeg, *Nat. Rev. Cancer*, 2016, **16**, 201.
53 X. He, H. Cao, H. Wang, T. Tan, H. Yu, P. Zhang, *Nano Lett*. 2017, **17**, 5546.

View Article Online
DOI: 10.1039/C9DT00506D

Graphical abstract

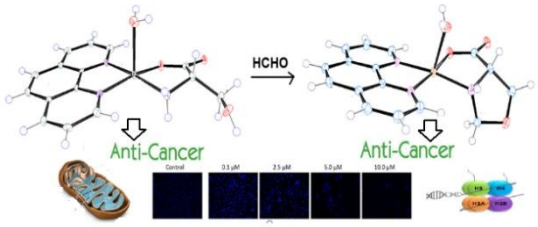

Chiral precursors and products, more potent than cisplatin, induced apoptosis *via* ROS production, massive drop in mitochondria membrane potential and epigenetic changes.